HHS Public Access

Author manuscript

Neuron. Author manuscript; available in PMC 2018 August 16.

Published in final edited form as:

Neuron. 2017 August 16; 95(4): 944–954.e4. doi:10.1016/j.neuron.2017.07.024.

Specialized mechanosensory nociceptors mediating rapid responses to hair-pull

Nima Ghitani[1,4], **Arnab Barik**[1,4], **Marcin Szczot**[1,4], **James H. Thompson**[1], **Chia Li**[2], **Claire E. Le Pichon**[3], **Michael J. Krashes**[2], and **Alexander T. Chesler**[1,5]

[1]National Institutes of Health (NIH), National Center for Complimentary and Integrative Health (NCCIH), Bethesda MD, USA

[2]National Institutes of Health (NIH), National Institute of Diabetes and Digestive and Kidney Diseases (NIDDK), Bethesda MD, USA

[3]National Institutes of Health (NIH), National Institute of Child Health and Human Development (NICHD), Bethesda MD, USA

SUMMARY

The somatosensory system provides animals with the ability to detect, distinguish and respond to diverse thermal, mechanical and irritating stimuli. While there has been progress in defining classes of neurons underlying temperature sensation and gentle touch, less is known about the neurons specific for mechanical pain. Here, we use in vivo functional imaging to identify a class of cutaneous sensory neurons that are selectively activated by high threshold mechanical stimulation (HTMRs). We show that their optogenetic excitation evokes rapid protective and avoidance behaviors. Unlike other nociceptors, these HTMRs are fast conducting Ad-fibers with highly specialized circumferential endings wrapping the base of individual hair follicles. Notably, we find that Ad-HTMRs innervate unique but overlapping fields and can be activated by stimuli as precise as the pulling of a single hair. Together the distinctive features of this class of Ad-HTMRs appear optimized for accurate and rapid localization of mechanical pain.

Keywords

Sensory coding; peripheral nervous system; mechanosensation; touch; nociception; pain

[5]Lead contact: alexander.chesler@nih.gov.

[4]these authors contributed equally to this work

AUTHOR CONTRIBUTIONS

N.G., A.B., M.S., and A.T.C. conceived the project. N.G. developed the in vivo preparation and performed the calcium imaging and single cell electrophysiology experiments. A.B. performed the anatomical and histological analyses. A.B. and C.L.P performed the in situ hybridization experiments. M.S. wrote the software for calcium imaging analyses and performed the optogenetic electrophysiological recordings. N.G., J.H.T., C.L., M.J.K. performed the behavioral tests. N.G., A.B., M.S., and A.T.C. analyzed and interpreted data. A.T.C. wrote the manuscript, with input from all authors.

Data and Software Availability

All data and custom made Matlab codes for calcium imaging analysis are available upon request.

INTRODUCTION

Peripheral sensory neurons innervating the skin provide animals with important details about their environment. For humans, the activity of these neurons is responsible for our sense of touch and evokes a range of emotional responses from pleasure to pain. Our understanding of how sensory neurons detect diverse stimuli is rooted in work from the late 19th century. In particular, Maximilian von Frey is credited with formalizing the idea that there are four sensations (touch, heat, cold, and pain), each detected by morphologically distinct receptor types (Norrsell et al., 1999). Von Frey posited that touch (including pressure and vibration) is detected by afferents with highly specialized endings (such as corpuscles and hair associated endings) while pain is sensed by afferents that make free nerve endings. This model has proved to be remarkably prescient. The past two decades have provided definitive links between specific classes of sensory neurons, the detection of particular stimuli and distinct afferent morphologies (Le Pichon and Chesler, 2014).

Perhaps the best example of sensory specificity is the activation of neurons expressing the heat gated ion channel Transient Receptor Potential Cation Channel Subfamily V Member 1 (Trpv1) by capsaicin (Caterina et al., 1997), which is sufficient to elicit the sensation of burning whereas the ablation of these neurons causes insensitivity to heat (Pogorzala et al., 2013). Genetic labeling of Trpv1-expressing neurons showed, just as predicted for “pain” sensation, that these neurons have free nerve endings in the superficial layers of skin (Cavanaugh et al., 2011). Similarly, molecular studies have also confirmed that low threshold mechanoreceptors (LTMRs) have specialized nerve endings with two distinct morphologies along the shaft of hair follicles, lanceolate endings running parallel to the hair shaft (Li et al., 2011), and circumferential endings wrapping around each hair follicle (Bai et al., 2015; Bardoni et al., 2014).

Despite these advances, decades of electrophysiological recordings have demonstrated the existence of populations of sensory neurons that remain poorly understood. These include several types of broadly tuned, polymodal neurons and, notably, classes of neurons that respond exclusively to high threshold mechanical stimuli (HTMRs) that are likely critically important for pain (Bessou and Perl, 1969; Schmidt et al., 1995). Furthermore, molecules commonly used to define classes of sensory neurons seem to target more than one subtype. For example, neurons that are immuno-positive for Calcitonin gene related peptide (CGRP) have long been classified as peptidergic nociceptors (Gibson et al., 1984). Ablation of neurons expressing Calca, one of two genes that encode CGRP, has shown that they are critical for thermosensation but not required for mechanical pain behaviors (McCoy et al., 2013). However, electrical recording from CGRP neurons demonstrated that many can respond to mechanical stimulation (Lawson et al., 2002; Weyer et al., 2015). Anatomical studies have also suggested CGRP neurons are likely heterogeneous. In hairy skin, CGRP-neurons have been shown to make free nerve endings typically associated with nociceptors, as well as circumferential endings that have been linked to touch (Bai et al., 2015; Bardoni et al., 2014).

We reasoned that new imaging approaches using genetically encoded calcium sensors (e.g. GCaMP6f) (Chen et al., 2013) would enable us to directly examine the tuning properties of

large populations of molecularly defined neurons (Emery et al., 2016; Smith-Edwards et al., 2016; Yarmolinsky et al., 2016) to uncover the existence of subclasses with specialized functions. Here, we use functional in vivo imaging to demonstrate that cutaneous Cacla neurons that project to hairy skin form two distinct groups: polymodal nociceptors and high threshold mechanoreceptors (that we call Circ-HTMRs). Notably, we show that Circ-HTMRs make highly specialized circumferential endings, are fast conducting and have spatially organized receptive fields – all attributes important for touch sensation. Yet robust activation of Circ-HTMRs results in immediate escape behaviors and rapidly conditions avoidance, showing these neurons function as nociceptors. These findings highlight unexpected morphological and functional properties of a class of Aδ-HTMRs that are distinct from c-fiber nociceptors and reveal conserved features underlying touch and pain sensation.

RESULTS

In vivo imaging reveals functional classes of sensory neurons

The trigeminal ganglion (TG) contains the cell bodies of sensory neurons which innervate peripheral targets including the head and neck. Mice could be surgically prepared such that the entire TG was exposed for in vivo imaging (see methods). Typically, we could record responses at single cell resolution from large fields (6.25 mm^2) containing hundreds to thousands of cells (Figure 1A–C). Moreover, this preparation was remarkably stable, allowing functional recordings to be carried out over a period of hours while stimulating the periphery (e.g. intact facial skin) with a wide range of sensory stimuli. Initially a genetic model was examined where a large subset of trigeminal neurons was targeted by crossing *Trpv1*-Cre (Cavanaugh et al., 2011) with conditional Rosa26-CAG-flox-Stop-GCaMP6f (Ai95D) (Madisen et al., 2015) to generate Trpv1-Cre; GCaMP6f mice ($Trpv1^{lin}$-GCaMP6f). Because Trpv1 is broadly expressed in developing trigeminal ganglion neurons (Cavanaugh et al., 2011; Mishra et al., 2011), we anticipated that functionally diverse neurons should express GCaMP6f.

As expected, $Trpv1^{lin}$-GCaMP6f neurons responded to a range of mechanical and thermal stimuli applied to the cheek (Figure 1C–E) including gentle touch (stroking with and against the grain of hairs), noxious mechanical stimuli (hair-pull) as well as heat and cold (Video 1). Neurons were functionally classified based on their selective activation by gentle or high threshold mechanical stimuli, heating or cooling, or as polymodal neurons that responded to both mechanical and thermal stimuli (Figure 1E). We confirmed that our ability to record diverse functional classes resulted from broad GCaMP6f expression by examining Trpv1-Cre mice crossed with a tdTomato reporter strain (Ai9; $Trpv1^{lin}$-tdT). Consistent with our functional recordings, approximately half the neurons in the trigeminal ganglion from $Trpv1^{lin}$-tdT mice expressed tdTomato. Expression was biased towards neurons with small and medium cell diameters (Figure S1A) (Cavanaugh et al., 2011; Mishra et al., 2011) that express markers for thermoreceptors (Trpv1 and Trpm8, S1D) (Caterina et al., 1999; McKemy et al., 2002; Peier et al., 2002), irritant receptors (Trpa1, S1D) (Jordt et al., 2004), mechano-nociceptors (MrgprD) (Zylka et al., 2005), and small diameter nociceptors (e.g. Npy2R, S1D) (Usoskin et al., 2015). Similarly, examination of hairy skin revealed two

prominent types of nerve endings; free nerve endings (Figure S1B) and lanceolate endings (Figure S1C). Overall our in vivo imaging approach was reliable, selective, and sensitive.

Functional imaging reveals distinct classes of cutaneous CGRP neurons

We next used an inducible *Calca* -Cre^{ERT2} driver line (Song et al., 2012) to selectively target expression of GCaMP6f in a subset of mature sensory neurons expressing the calcitonin gene related peptide (Calca-GCaMP6f). The neuropeptide CGRP is expressed in about 30% of sensory neurons and is important for pain, vascular control and neuroinflammation (McCoy et al., 2012; Russell et al., 2014). However, ablation studies indicate that Calca-expressing neurons may have a particular role in thermosensation (McCoy et al., 2013). Interestingly, our imaging studies (Figure 2) revealed that Calca-neurons innervating hairy skin of the cheek fall into three broad classes of neurons responding to: heat (31% to >40°C), high threshold mechanical stimulation (44% to hair-pull,), or to both (25%, Figure 2B–C, Video 2). Calca neurons were insensitive to lower threshold mechanical stimuli (air puff, brushing, or stroking; Figure S2; Video 2), showing they are not involved in gentle touch sensation. Moreover, we did not observe significant activation by either warm temperatures (<37°C) or by cooling (>13°C; Figure S2B). These findings generalized to sensory neurons innervating other types of hairy skin. Similar in-vivo imaging experiments in the Dorsal Root Ganglia (DRG) in the lumbar region showed similar high threshold mechanical sensitivity of CGRP neurons innervating the hind leg (Figure S2C).

Sorting responses of Calca-neurons by soma diameter revealed that heat sensitive neurons were smaller than the heat insensitive neurons (17±2 μm for heat sensitive and 26±6 μm for mechanosensitive; Figure 2C, S2A). We next generated mice where Calca-neurons express tdTomato by crossing the *Calca*-Cre^{ERT2} strain with Ai9-reporter mice (Calca-tdT; (Madisen et al., 2010). Two color in-situ hybridization demonstrated that nearly all Calca expressing neurons were tdTomato-positive (78± 8%). We found that *Trpv1* was expressed in the small diameter *tdTomato*-positive neurons and excluded from larger diameter neurons (Figure S3A) (McCoy et al., 2013; McCoy et al., 2012; Mishra et al., 2011). Intriguingly, larger Calca-HTMRs did not conform to previously described types of mechanoreceptor as they lacked expression of markers previously ascribed to LTMRS (Ntrk2, Ntrk3, TH, MrgprB4) and nociceptors (TrpA1, MrgprD; Figure S3D) (Bardoni et al., 2014; Li et al., 2011; Vrontou et al., 2013; Zylka et al., 2005). We found limited overlap with Npy2R (<20%), suggesting the majority of larger Calca neurons also lack this marker (Arcourt et al., 2017; Li et al., 2011; Usoskin et al., 2015). Our data reveal that Calca neurons innervating hairy skin fall into two anatomical classes: small, heat sensitive neurons that express Trpv1 and a previously undescribed class of HTMRs (Figures S4–S5).

Medium diameter Calca-neurons are HTMRs that make circumferential endings

Intersectional approaches are useful for separating groups of neurons within a larger population (Huang and Zeng, 2013). Resiniferatoxin (RTX) is a potent Trpv1 agonist that effectively kills neurons expressing this receptor (Cavanaugh et al., 2011; Olah et al., 2001). We reasoned that because Trpv1 is expressed in heat-sensitive Calca neurons but not in the larger HTMRs, we might be able to use RTX ablation to study these mechanosensors. As expected, repeated systemic dosing of neonatal mice with RTX depleted the TG and DRG of

TRPV1-expressing cells while sparing the larger diameter Calca neurons (Figure S4 and Figure S5). Importantly, functional imaging revealed that RTX administration resulted in the near complete loss of temperature-sensitive neurons (Figure 3A–C, S4, Video 3). In contrast, the HTMRs were unaffected by RTX treatment (Figures 3A–C, S4, Video 3). These tests established a chemical-genetic strategy to selectively study the anatomy and functional properties of Calca-expressing HTMRs.

Typically, thermoreceptors (Cavanaugh et al., 2011) and HTMRs (Arcourt et al., 2017) are known to make free nerve endings in skin whereas myelinated touch neurons have specialized endings often related to their unique functional specificities (Abraira and Ginty, 2013; Arcourt et al., 2017; Bardoni et al., 2014). Interestingly, it has been reported that CGRP-neurons make both types of sensory projections to the skin (Bai et al., 2015; Bardoni et al., 2014), free nerve endings and a more complex “lasso-like” circumferential ending associated with each hair follicle. The latter was in many ways similar to the circumferential endings described for a class of touch neurons called field-Low Threshold Mechanoreceptors (field-LTMRs) with the notable exception that CGRP endings did not stain with NF200, a reliable marker for A-fiber neurons (Bai et al., 2015). To study the sensory terminals of Calca-HTMRs we examined skin from *Calca*-Cre^{ERT2} mice crossed with Ai9-reporter strain (Calca-tdT) (Madisen et al., 2010). Free nerve endings in superficial layers of skin and circumferential endings associated with each hair were tdT-positive (Figure 2E–F). However, no reporter expression was observed in skin cells including Merkel cells (Figure S6A). Calca innervation in hairy skin from cheek, belly and back (innervated by the TG or DRG) was indistinguishable (Figure S6B and S7A). Furthermore, tdTomato afferents are NF200 negative demonstrating these endings are distinct from a recently identified class of HTMR (Figure S6C) (Arcourt et al., 2017).

We treated Calca-tdT mice with RTX to ablate heat-sensitive neurons. Notably, circumferential endings resisted RTX ablation (Figure 3D–E; Figure S7A–B). In contrast, free nerve endings, which were prominent in Calca-tdT mice, were eliminated by RTX treatment (Figure 3D; Figure S7). Thus, we chose to call these cells “Circ-HTMRs” to highlight that their response properties are reminiscent of nociceptors but they have sensory specializations normally associated with neurons involved in touch. Notably, a recent study identified a population of fast-conducting HTMRs using a different genetic strategy (Arcourt et al., 2017). Unlike the Circ-HTMRs studied here, these neurons had free nerve endings that were NF200-positive but also appeared positive for CGRP. Importantly, Circ-HTMRs projecting to the skin were never NF200 positive (Figure S6C), and free nerve endings were not observed after RTX ablation (Figure 3D–E; Figure S7). Therefore, the Circ-HTMRs are distinct from the neurons identified by Arcourt et al. (2017) and Calca-CreER recombination does not label these neurons.

Optogenetic activation of Circ-HTMRs reveals they are nociceptors

A defining feature of nociceptors is that their activation is sufficient to evoke protective reflexes and behaviors (Daou et al., 2013). Therefore, to directly determine whether Circ-HTMRs are nociceptors we selectively expressed channelrhodopsin-2 (ChR2) in these neurons (Calca-cre ^{ERT2} X Rosa26-CAG-ChR2), and examined behavioral responses to

optogenetic stimulation in mice treated with RTX; Figures 4). As a control, we confirmed that these mice were insensitive to heat (Figure 4A) verifying that they lacked Trpv1 nociceptors. Furthermore, examination of hairy skin showed that ChR2 protein was found in circumferential endings (Figure 4B). A flash of blue light on the hairy skin of freely moving Calca-ChR2-RTX mice elicited a rapid withdrawal response (Figure 4D). Blue light evoked immediate flinching and jumping responses within milliseconds of stimulation that were never seen in response to red light or in control mice. The magnitude of behavioral responses was proportional to light intensity (Figure 4D). Repeated stimulation caused mice to develop nocifensive/guarding postures (hunching). Notably, rapid escape behaviors could be elicited by sweeping a spot of blue light across their backs and heads, something not seen with red light or in controls. This type of optical stimulation was sufficient to cause rapid avoidance of a light-paired chamber, whether mice were stimulated on their back (Figure 4D–E) or top of the head (Figure 4F). Thus, selective activation of Circ-HTMRs is strongly aversive, demonstrating the nociceptive phenotype of these neurons.

Circ-HTMRs are Aδ-mechano-nociceptors

We noticed that the speed with which mice reacted to light stimulation was remarkably fast. We observed the belly begin recoiling from the fiber within ~22 milliseconds from the onset of light (21.63 ± 1.4 std, n=5 animals repeated at least 20 times per animal). The majority of classes of nociceptors are slowly conducting C-fibers, but fast Ad-fibers have also been shown to respond to high threshold stimuli (Brown and Iggo, 1967; Burgess and Perl, 1967; Leem et al., 1993). Interestingly, over half a century ago Burgess and Perl (1967) described fast responding neurons from cats that responded to hair pull (Burgess and Perl, 1967). We wondered if the Circ-HTMRs were a similar type of fast-conducting mechanical nociceptor. To test this hypothesis, we measured conduction velocities (CVs) from Circ-HTMRs in the DRG by performing extracellular sharp electrode recordings of action potentials (APs) triggered by electrical stimulation of hairy skin (Figure 5A–E). These experiments were simultaneously performed with calcium imaging to target neurons responsive to the site of stimulation (Figure 5A). Interestingly, we found that single action potentials could be reliably reported by GCaMP6f signals with high fidelity (Figure 5B). We found that small diameter Calca neurons (19.8 ± 1.5 mm, n=6) had an average CV in the C-fiber range (0.71 ± 0.13 m/s), while medium diameter Calca neurons (34.8 ± 2.2 mm, n=6) had an average CV in the Aδ range (means: 3.6 ± 0.47 m/s) (Figure 5C–D). Additionally, we measured CVs in the Aδ range in RTX treated Calca-ChR2 mice from evoked compound action potentials in the exposed sciatic nerve using optogenetic stimulation of hairy skin (means: 5.87 ± 0.44 m/sec, n=5). Thus Circ-HTMRs have the response tuning (Figure 3A–C), biophysical properties (Figure 5C–D) and the specialized sensory endings (Figure 3D–E) that might be expected for hair-pull neurons (Burgess and Perl, 1967).

Circ-HTMRs have sustained responses to single hair pull and have partially overlapping receptive fields

To further define the response properties of Circ-HTMRs, we examined their responses to a panel of high threshold mechanical stimuli. Circ-HTMRs could be activated by pinching the skin (Figure 6A and C) as well as by stiff punctate stimuli (von Frey filaments >4 mN; Figure 6B–D). Notably, sustained mechanical stimulation produced sustained responses

(>10 s; Figure 6A–C). The threshold for activation was measured by repeated stimulation of the receptive field with von Frey filaments calibrated at different forces. Circ-HTMRs required forces in excess of 4.0 mN for activation, similar in what we found for HTMRs labeled in $Trpv1^{lin}$-GCaMP6f mice. The threshold for activation was much less sensitive than for LTMRs, that we found reliably activated with forces as little as 0.7 mN (Figure 6D). Therefore, Circ-HTMRs are slowly adapting mechano-nociceptors that can be activated by multiple types of high threshold stimuli. Remarkably, pulling a single guard hair reliably activated a small but reproducible group of Circ-HTMRs (<10 neurons/field of view; Figure 7A–C).

The sensation of mechanical pain results in rapid behaviors that include protecting and tending to an affected area. We were intrigued by the fact that Circ-HTMRs were activated by distinct combinations of single hairs (Figure 7B). These results suggested that spatial encoding of mechanical pain might use a similar combinatorial strategy to the one proposed for gentle touch (Abraira and Ginty, 2013). We therefore mapped the receptive fields of multiple Circ-HTMRs from the same mouse to determine the size and extent of overlap between individual receptive fields. High threshold von Frey stimulations (10 mN) were applied across dozens of sites on the cheek to map the receptive fields of large populations of single neurons from any mouse (Figure 7D). Circ-HTMRs generally have relatively large receptive fields (Figure 7E), similar in size to other sensory neuron types making circumferential endings (Bai et al., 2015; Wu et al., 2012). Receptive field size correlated with cell diameter (Figure 7G). Large receptive fields typically contained non-responsive patches surrounded by areas showing high sensitivity (Figure 7F). Notably, Circ-HTMRs had partially overlapping receptive fields tiled across the cheek (Figure 7D). Since having a single hair pulled evokes sharp, localized, sustained pain, Circ-HTMR activation seems ideally suited to encoding these features.

DISCUSSION

The past two decades have seen a number of advances in the genetic and functional dissection of the neurons for temperature, itch, and touch sensation (Le Pichon and Chesler, 2014). To date, most studies on nociception have focused on the unmyelinated C-fibers. Meanwhile, our understanding of Aδ-nociceptors remained much less complete. Here we provide evidence that a subset of cutaneous Calcaneurons that lack TRPV1 expression are Aδ-HMTRs. We established a chemical-genetic intersectional approach to allow us to ascertain their tuning properties, morphology, and function.

Using in vivo functional imaging, we demonstrated that sensory neurons expressing Calca and innervating hairy skin respond to noxious mechanical and thermal stimuli. Previously it was shown that ablation of the Calca-neurons resulted in marked thermal deficits but not significant mechanosensory impairment (McCoy et al., 2013) perhaps because their studies focused on glabrous skin which lacks Circ-HTMRs. Our finding that a large subset of Calca neurons that innervate hairy skin are activated by high-threshold mechanical stimuli highlights that, unlike thermosensation, mechanosensation is likely encoded by sensory populations with overlapping functions. This may be a general explanation for why early electrophysiological data highlighted an abundance of polymodal fibers whereas recent

genetic studies have suggested narrow tuning. Indeed, we find that vast majority of small diameter neurons co-expressing Trpv1 and Calca are polymodal nociceptors rather than thermoreceptors.

Half a century ago Burgess and Perl (1967) recorded HTMRs in cats that innervated hairy skin and were fast conducting and subsequently found similar neurons in primates (Perl 1968). We find that Circ-HTMRs share all of the features described in these classic studies including conduction velocity, insensitivity to temperature, large receptive fields made up of punctate hot spots, and slow adaptation. Unexpectedly, these Aδ-mechanoreceptors do not make the free nerve endings typical of nociceptors but rather circumferential endings that are structurally similar to those made by field-LTMRs (Bai et al., 2015). However, despite a shared morphology, field-LTMRs respond to a wide range of stimuli from gentle stroking to high threshold mechanical activation while Circ-HMTRs respond only to noxious mechanical stimuli such as hair pull. Thus, neurons with circumferential endings may all respond to hair pull but Circ-HMTRs appear specialized to transmit only noxious responses.

Interestingly a recent study using a different molecular strategy identified a population of Aδ-mechano-nociceptors that innervate the skin (Arcourt et al., 2017). These neurons form NF200-positive free nerve endings in superficial layers of the skin and are morphologically distinct from the Circ-HMTRs that we identify here. Whereas the neurons identified by Arcourt et al. (2017) have all the features expected for nociceptors, the unique structure of Circ-HTMRs and the fact that each hair has such endings insinuate a highly specialized protective role.

Our chemical-genetic intersectional strategy has allowed us to discern three key principles for Circ-HTMRs. First we show that these Aδ-mechano-nociceptors have sustained responses and are sensitive to the pulling of even a single hair. Second, we show that noxious activation of each hair is detected by a small cluster of Circ-HTMRs with partially overlapping receptive fields. Notably, the tiling of their inputs across the skin suggests that they convey spatial information. Third, we demonstrate that activation of Circ-HTMRs evokes fast and robust protective behaviors and quickly promotes avoidance. These features are exactly those expected for the rapid detection and precise localization of potential tissue damage such as hair pull.

Future studies can leverage the chemical-genetic approach developed here to study Aδ-HTMR connectivity in the spinal cord and neural circuits activated by noxious mechanical stimuli in the brain. Furthermore, deciphering the response properties of different classes of mechanical nociceptors should ultimately help explain how humans can distinguish and respond appropriately to a wide variety of different types of painful touch. Our results highlight the remarkable specialization that exists between classes of nociceptors and mechanoreceptors. Understanding the molecular mechanisms underlying these different types of responses will be an important step toward the rational design of new approaches to pain therapy.

STAR Methods

Contact for Reagents and Resource Sharing

Additional information and requests for reagents and other resources should be made to, and will be fulfilled by the Lead Contact, Alexander Chesler (alexander.chesler@nih.gov).

Experimental Model and Subject Details

All animal care and experimental procedures were performed in accordance with a protocol approved by the National Institute of Health Animal Care and Use Committee. TRPV1-Cre or B6.129-TRPV1$^{tm1(cre)Bbm/J}$ (Stock number 017769); Rosa-LSL-tdTomato or B6.129S-Gt(ROSA)$^{tm66.1(CAG-tdTomato)Hze/J}$ or Ai9 (Stock number 005975); Rosa-LSL-GCaMP6f or B6J.Cg-*Gt(ROSA)26Sor*$^{tm95.1(CAG-GCaMP6f)\ Hze/MwarJ}$ or Ai95D (Stock number 028865) strains were purchased from Jackson Laboratories (Cavanaugh et al., 2011; Madisen et al., 2015; Madisen et al., 2010). *Calca*-cre^{ERT2} was generously provided by Dr. Pao-Tien Chuang (Cardiovascular Research Institute, University of California, San Francisco, CA) (Song et al., 2012). Mice of both sexes were used in all experiments. Genotyping was performed according to information provided by Jackson Laboratories.

Cre induction—Cre activity was induced by tamoxifen (TMX), administered twice by intraperitoneal injection at 100 mg/kg body weight at three weeks of age and older. Injections were spaced by three days for recovery. Mice were used in experiments after at least one week post tamoxifen injection.

RTX treatment—Pups at 3–5 days old were injected intraperitoneally with 50 μl of 20 μM Resiniferatoxin (RTX), and with double the dose on each successive day to a final dose of 80 μM. Adult mice treated with RTX as pups were again re-dosed with RTX (final dose level) prior to use in behavioral or imaging experiments.

Method Details

Multiplex fluorescent in-situ hybridization (ISH)—Fresh TGs and DRGs were harvested from mice and rapidly frozen over dry ice. The tissues were embedded in OCT (Tissue-Tek) and sectioned on a cryostat. 16 μm sections were mounted on charged glass slides (Daigger Scientific). Multiplex ISH was done with the manual RNAscope assay (Advanced Cell Diagnostics)

Immunostaining—Hair from the skin of the back of mice was removed using a depilatory cream (Nair), and cut into square pieces of approximately 5 mm × 5 mm. The tissues were fixed in 4% PFA (Electron Microscopy Sciences) in PBS at 4 °C for 3–5 days. After a PBS wash, tissues were mounted in OCT medium (Tissue Tek), and sectioned at 80–90 μm on a cryostat (Leica). Skin sections were rinsed in PBS and incubated in blocking buffer (5% goat serum; 0.5% Triton-X100) for 3 hours at room temperature. Sections were incubated in primary antibodies (chicken anti-NF200, Aves labs; rabbit anti-RFP, Rockland) in blocking buffer at 4°C overnight. Sections were rinsed and incubated overnight in AlexaFluor conjugated secondary antibodies (Thermofisher Scientific), washed in PBS, and mounted in ProLong gold mounting media (Thermofisher Scientific). Z-stack images were collected

using a 40X oil objective on a laser scanning confocal system (Olympus Fluoview FV1000), and processed using ImageJ/FIJI software (National Institutes of Health).

Trigeminal Ganglion Imaging Preperation—Mice of either sex at 4–8 weeks were anesthetized with inhalational Isoflurane/Oxygen mix and positioned in a custom built stereotactic frame with heads fixed using ear and tooth bars. Continuous flow of isoflurane/Oxygen was provided through a nosepiece. A hand warmer was placed under the mouse to stabilize body temperature. With the aid of a dissecting stereoscope (Leica), a small strip of skin (2×10 mm) on top of the head was removed and the skull exposed. Connective tissue on the exposed skull was removed using cotton tipped applicators. A round opening in the cranium (~7 mm in diameter, centered at Bregma) was made using a dental drill (Ideal micro drill, Cellpoint scientific), and the dura was cut using surgical scissors. A glass Pasteur pipette, pulled at the tip to an inner diameter of ~500 μm, bent at a 70–90 angle, and under vacuum suction, was used to carefully aspirate the forebrain to expose the left and right TGs. The cranium was repeatedly washed and bathed in HEPES buffer (in mM: 160 NaCl, 6 KCl, 13 Glucose, 13 HEPES, 2.5 CaCl2, 2.5 $MgCl_2$, and pH adjusted to 7.2 with 10N NaOH). Excessive bleeding was controlled using Gelfoam dental sponges (Pfizer). A rubber o-ring (9 mm diameter, RT Dygert) was glued over the opening on the skull using a cyanoacrylate based adhesive. A custom-made stabilization bar securely mounted to the frame was attached to the o-ring and skull using dental cement.

Dorsal Root Ganglion Imaging Preparation—Mice were positioned in a custom stereotactic frame under anesthesia as above. The hair on the back was shaved, and a sagittal incision was made over the lumbar vertebrae. Muscle and connective tissues were carefully remove, avoiding damage to the peripheral nerves. The vertebrae were stabilized at two sites using surgical clamps (Kopf). A dental drill was used to cut an opening in the bone of the lumbar vertebrae covering a DRG on the left side. Forceps were used to carefully pull away bone cut by the dental drill, to expose the DRG. HEPES buffer was used continuously to wash and hydrate the DRG. Excessive bleeding was controlled using Gelfoam sponges, and with application of Trombin (Sigma).

Calcium Imaging—The surgical preparation was transferred on the stage of an epifluorescence microscope (MPERS, Olympus) equipped with a 4X, 0.28 NA air objective. Illumination was provided with a 130 W halogen light source (U-HGLGPS, Olympus), using a standard green excitation/emission filter cube. Imaging was performed using an Orca Flash 4.0 CMOS camera (Hamamatsu), in trials lasting 40 s, at a 5 Hz frame rate, using Metamorph image acquisition software.

Combined electrical and calcium recordings in the DRG—Our calcium imaging system with a 20X, 0.40 NA air objective was used to identify responsive neurons to mechanical and electrical stimuli (30–70 volts, 400 μs) delivered to the skin. Sharp micropipettes were fabricated from quartz glass capillaries using a P 2000 puller (Sutter Instruments) and filled with 3M KCl, with a resistance of 80 MΩ. Pipettes were coupled to an Multiclamp700B amplifier headstage (Molecular Devices). A motorized micromanipulator (Sutter Instruments) was used to position pipettes to cells of interest under

visual guidance. Extracellular spikes and GCaMP6f signals were acquired simultaneously. Spikes were digitized at 10 KHz (Digidata 1550) and acquired using pClamp software (Molecular Devices). Synchronization of calcium imaging and spike recordings, and delivery of electrical stimulation to the skin was controlled by pClamp software and Digidata 1550. Conduction velocities were measured for each neuron, by dividing distance (site of stimulation to DRG) by the latency to response.

Mechanical Stimulation and Videography—Gentle stroking of the mouse cheek, with and against the grain of the hairs, was performed manually using cotton tipped applicators. Special care was taken to maintain each stroke consistent at ~10–15 mN of applied force. Hair pull and skin pinch was performed using forceps. Gentle air puff was made using a Picospritzer III (Parker), with a custom air nozzle positioned 2.5 cm from the cheek. Video recordings were performed on all trials with mechanical stimulations using a CMOS video camera (acA2000-165um, Basler), and a 0.6X telecentric lens (Edmunds Optics). For single hair pull experiments, a fine forceps and a 1X telecenric lens was used. A trigger pulse generated by Digidata 1550 and controlled by Clampex 10 software (Molecular Devices) initiated video recordings and calcium imaging synchronously.

Temperature Stimulation—Temperature ramps were applied to the mouse cheek using a custom-built apparatus, consisting of three M3 Lauda bath recirculators (Lauda Brinkmann), set to cold, hot, and room temperatures, pumping water through a series of solenoid pinch valves (NResearch Incorporated) which direct water through a copper thermode. Trigger pulses generated by the Digidata 1550 and Clampex controlled shutting on and off of pinch valves, which produced the rise and fall of the temperature ramps. A digital thermometer attached to the copper thermode measured the temperature ramps as an analogue input to Digidata 1550 and was recorded using Clampex.

von Frey Mapping—The hairs on the mouse cheek were trimmed using a small hair clipper (Wahl), then removed completely using a hair removal cream (Nair). A 10 mN von Frey filament was used to make localized mechanical stimulations, randomly distributed within the confines of the depilated cheek, while simultaneously recording calcium signals and video of the stimulations. Mapping data were analyzed using custom written Matlab scripts (Mathworks). To compare relative sizes of mapped receptive fields we calculated the minimum weight spanning tree connecting all responsive points, and total tree length was used as a measure of receptive field extensity. To visualize responsive area boundaries, nonconvex polygon vertices encompassing all responsive points were calculated.

Conduction Velocity (CV) measurement from compound action potentials—Adult mice were anesthetized with inhalational Isoflurane/Oxygen mix and positioned on the heating pad dorsal side up. Hind paws were gently stretched and immobilized with adhesive tape. Hair on the lower part of the trunk and hind paws was shaved and depilated to expose skin. A rectangular patch of the skin was excised to expose the gluteus maximus and external oblique muscles, which were gently retracted to visualize a 6–8 mm stretch of the sciatic nerve. The sciatic nerve was continuously bathed in ACSF.

Compound action potentials (CAPs) were recorded with an ACSF-filled pipette suction electrode connected to a headstage of a Multiclamp700B amplifier. The electrode was positioned over the nerve at a steep angle (~80°) and negative pressure was applied to form a tight contact between pipette and nerve. CAPs were evoked by optogenetic stimulation of the intact thigh skin, using a blue fiber-coupled LED (Prizmatix) with the fiber tip positioned ~1–2 mm from the skin. A 1 ms command pulse was used to drive light stimulation with peak optical power of 37 mW. Stimulation was controlled with Clampex 10 software through Digidata 1550 acquisition system. For each site, stimulation was repeated >90 times, data presented are averaged responses. 50 Hz electrical interference was filtered offline. To calculate the CV, the distance between stimulation and recording sites was measured and divided by response latency.

Behavioral Measurements—For behavioral testing with optogenetics, a strip of skin along the backs or bellies of RTX ablated Calca-ChR2 and age matched Calca-GCaMP6f mice (as controls) was shaved and depilated a day before testing to allow blue light to efficiently reach the skin. Using a fiber coupled LED (Prizmatix), the fiber tip was manually positioned within 6–8 mm of the belly and the LED was switched on while performing high speed (120 fps) video of the behavior. The mouse response to blue light stimulation at different power intensities was scored as described in Fig 4. For the Real Time Place Aversion (RTPA) assay, mice were placed in a cage with two chambers separated by a wall with a round opening in the center, allowing mice to freely explore both chambers. Using a magnifying lens and the Prizmatix blue LED, light was focused on the depilated backs of mice when they entered one chamber but not the other. Mouse movement was video recorded and automatically tracked offline using CleverSys software.

Quantification and Statistical Analysis

Calcium Imaging Analysis—Calcium imaging stacks across multiple trials representing all applied stimuli were concatenated for each animal to generate a single tiff stack using ImageJ. Tiff stacks were corrected for movement artifact using the Linear Stack Alignment plugin in ImageJ. Regions of interest (ROIs) were selected manually in ImageJ using the Cell Magic Wand plugin. A total of 213 responsive Trpv1^{lin}-GCaMP6f TG (n = 213 neurons in 3 animals; see Figure 1), 430 responsive Calca-GCaMP6f TG neurons (n = 430 neurons from 15 animals; see Figure S2), 136 Calca-GCaMP6f TG neurons from animals treated with RTX (n = 136 neurons from 5 animals; see Figure 3), and 52 Calca-GCaMP6f DRG neurons (n = 52 neurons form 3 animals, see Figure S2) were analyzed.

ROI signal analysis was performed using custom written Matlab scripts (Mathworks). For $\Delta f/F_0$ determination F_0 was calculated as an average of 5 frames with lowest F from each stack of 200 frames. Custom written Matlab scripts were used for neuropil subtraction: fluorescence signals of a donut shaped area around each ROI were subtracted from the cell response to remove possible contribution of out of focus signal. Neurons were assigned as responsive to any given stimuli if dF/F_0>20%. Cells were qualified as mechano-, heat- or mechano-heat-responsive based on unbiased classification by a K-means clustering algorithm with assumed cluster numbers equal to 3. Clustering centroids obtained from

analysis of Calca-GCAMP6f results were used to classify responses in Calca-GCAMP6f RTX-treated mice.

Quantification of Histology—Co-expression of $Trpv1^{lin}$-tdT with sensory neuron markers was quantified for label overlap using ImageJ. For each experiment, representative confocal images from tissue sections were quantified (n = 5 sections from 3 animals). Co-expression of *tdTomato* with sensory neuron markers are quantified for label overlap using ImageJ (n = 5 sections from 3 animals). Quantification of hair shafts with circumferential endings was performed in ImageJ from confocal images (n = 10 skin preparations from 3 animals). To quantify the lengths of free nerve endings, a line was traced using the free hand tool of ImageJ, and the absolute length was measured (n = 10 skin preparations from 3 animals)

Supplementary Material

Refer to Web version on PubMed Central for supplementary material.

Acknowledgments

We are indebted to Nick Ryba and Mark Hoon (NIDCR) for their invaluable advice. Eileen Nguyen, Ruby Lam, Hanna Silberberg, and Latoya Hyson (NCCIH) provided assistance. We thank Mark Stopfer (NICHD) for assistance with single cell electrical recordings. We thank David Ide, Bruce Pritchard, Tom Talbot, Danny Trang, Phuoc Pham, Daniel Yochelson, and George Dold at the NIH Section on Instrumentation for design and fabrication of custom built instruments used in this study. We thank Pao-Tien Chuang (UCSF) for providing the Calca-CRE^{ERT2} mice and the GENIE project for the development of GCaMP6. This work was supported by the Intramural Research Program of the NIH, National Center for Complimentary and Integrative Health (ATC).

References

Abraira VE, Ginty DD. The sensory neurons of touch. Neuron. 2013; 79:618–639. [PubMed: 23972592]

Arcourt A, Gorham L, Dhandapani R, Prato V, Taberner FJ, Wende H, Gangadharan V, Birchmeier C, Heppenstall PA, Lechner SG. Touch Receptor-Derived Sensory Information Alleviates Acute Pain Signaling and Fine-Tunes Nociceptive Reflex Coordination. Neuron. 2017; 93:179–193. [PubMed: 27989460]

Bai L, Lehnert BP, Liu J, Neubarth NL, Dickendesher TL, Nwe PH, Cassidy C, Woodbury CJ, Ginty DD. Genetic Identification of an Expansive Mechanoreceptor Sensitive to Skin Stroking. Cell. 2015; 163:1783–1795. [PubMed: 26687362]

Bardoni R, Tawfik VL, Wang D, Francois A, Solorzano C, Shuster SA, Choudhury P, Betelli C, Cassidy C, Smith K, et al. Delta opioid receptors presynaptically regulate cutaneous mechanosensory neuron input to the spinal cord dorsal horn. Neuron. 2014; 81:1312–1327. [PubMed: 24583022]

Bessou P, Perl ER. Response of cutaneous sensory units with unmyelinated fibers to noxious stimuli. J Neurophysiol. 1969; 32:1025–1043. [PubMed: 5347705]

Brown AG, Iggo A. A quantitative study of cutaneous receptors and afferent fibres in the cat and rabbit. J Physiol. 1967; 193:707–733. [PubMed: 16992307]

Burgess PR, Perl ER. Myelinated afferent fibres responding specifically to noxious stimulation of the skin. J Physiol. 1967; 190:541–562. [PubMed: 6051786]

Caterina MJ, Rosen TA, Tominaga M, Brake AJ, Julius D. A capsaicin-receptor homologue with a high threshold for noxious heat. Nature. 1999; 398:436–441. [PubMed: 10201375]

Caterina MJ, Schumacher MA, Tominaga M, Rosen TA, Levine JD, Julius D. The capsaicin receptor: a heat-activated ion channel in the pain pathway. Nature. 1997; 389:816–824. [PubMed: 9349813]

Cavanaugh DJ, Chesler AT, Braz JM, Shah NM, Julius D, Basbaum AI. Restriction of transient receptor potential vanilloid-1 to the peptidergic subset of primary afferent neurons follows its developmental downregulation in nonpeptidergic neurons. J Neurosci. 2011; 31:10119–10127. [PubMed: 21752988]

Chen TW, Wardill TJ, Sun Y, Pulver SR, Renninger SL, Baohan A, Schreiter ER, Kerr RA, Orger MB, Jayaraman V, et al. Ultrasensitive fluorescent proteins for imaging neuronal activity. Nature. 2013; 499:295–300. [PubMed: 23868258]

Daou I, Tuttle AH, Longo G, Wieskopf JS, Bonin RP, Ase AR, Wood JN, De Koninck Y, Ribeiro-da-Silva A, Mogil JS, et al. Remote optogenetic activation and sensitization of pain pathways in freely moving mice. J Neurosci. 2013; 33:18631–18640. [PubMed: 24259584]

Emery EC, Luiz AP, Sikandar S, Magnusdottir R, Dong X, Wood JN. In vivo characterization of distinct modality-specific subsets of somatosensory neurons using GCaMP. Sci Adv. 2016; 2:e1600990. [PubMed: 27847865]

Gibson SJ, Polak JM, Bloom SR, Sabate IM, Mulderry PM, Ghatei MA, Mcgregor GP, Morrison JFB, Kelly JS, Evans RM, et al. Calcitonin Gene-Related Peptide Immunoreactivity in the Spinal-Cord of Man and of 8 Other Species. Journal of Neuroscience. 1984; 4:3101–3111. [PubMed: 6209366]

Huang ZJ, Zeng H. Genetic approaches to neural circuits in the mouse. Annu Rev Neurosci. 2013; 36:183–215. [PubMed: 23682658]

Jordt SE, Bautista DM, Chuang HH, McKemy DD, Zygmunt PM, Hogestatt ED, Meng ID, Julius D. Mustard oils and cannabinoids excite sensory nerve fibres through the TRP channel ANKTM1. Nature. 2004; 427:260–265. [PubMed: 14712238]

Lawson SN, Crepps B, Perl ER. Calcitonin gene-related peptide immunoreactivity and afferent receptive properties of dorsal root ganglion neurones in guineapigs. J Physiol. 2002; 540:989–1002. [PubMed: 11986384]

Le Pichon CE, Chesler AT. The functional and anatomical dissection of somatosensory subpopulations using mouse genetics. Front Neuroanat. 2014; 8:21. [PubMed: 24795573]

Leem JW, Willis WD, Chung JM. Cutaneous sensory receptors in the rat foot. J Neurophysiol. 1993; 69:1684–1699. [PubMed: 8509832]

Li L, Rutlin M, Abraira VE, Cassidy C, Kus L, Gong S, Jankowski MP, Luo W, Heintz N, Koerber HR, et al. The functional organization of cutaneous low-threshold mechanosensory neurons. Cell. 2011; 147:1615–1627. [PubMed: 22196735]

Madisen L, Garner AR, Shimaoka D, Chuong AS, Klapoetke NC, Li L, van der Bourg A, Niino Y, Egolf L, Monetti C, et al. Transgenic mice for intersectional targeting of neural sensors and effectors with high specificity and performance. Neuron. 2015; 85:942–958. [PubMed: 25741722]

Madisen L, Zwingman TA, Sunkin SM, Oh SW, Zariwala HA, Gu H, Ng LL, Palmiter RD, Hawrylycz MJ, Jones AR, et al. A robust and high-throughput Cre reporting and characterization system for the whole mouse brain. Nat Neurosci. 2010; 13:133–140. [PubMed: 20023653]

McCoy ES, Taylor-Blake B, Street SE, Pribisko AL, Zheng J, Zylka MJ. Peptidergic CGRPalpha primary sensory neurons encode heat and itch and tonically suppress sensitivity to cold. Neuron. 2013; 78:138–151. [PubMed: 23523592]

McCoy ES, Taylor-Blake B, Zylka MJ. CGRPalpha-expressing sensory neurons respond to stimuli that evoke sensations of pain and itch. PLoS One. 2012; 7:e36355. [PubMed: 22563493]

McKemy DD, Neuhausser WM, Julius D. Identification of a cold receptor reveals a general role for TRP channels in thermosensation. Nature. 2002; 416:52–58. [PubMed: 11882888]

Mishra SK, Tisel SM, Orestes P, Bhangoo SK, Hoon MA. TRPV1-lineage neurons are required for thermal sensation. EMBO J. 2011; 30:582–593. [PubMed: 21139565]

Norrsell U, Finger S, Lajonchere C. Cutaneous sensory spots and the “law of specific nerve energies”: history and development of ideas. Brain Res Bull. 1999; 48:457–465. [PubMed: 10372506]

Olah Z, Szabo T, Karai L, Hough C, Fields RD, Caudle RM, Blumberg PM, Iadarola MJ. Ligand-induced dynamic membrane changes and cell deletion conferred by vanilloid receptor 1. J Biol Chem. 2001; 276:11021–11030. [PubMed: 11124944]

Peier AM, Moqrich A, Hergarden AC, Reeve AJ, Andersson DA, Story GM, Earley TJ, Dragoni I, McIntyre P, Bevan S, et al. A TRP channel that senses cold stimuli and menthol. Cell. 2002; 108:705–715. [PubMed: 11893340]

Pogorzala LA, Mishra SK, Hoon MA. The cellular code for mammalian thermosensation. J Neurosci. 2013; 33:5533–5541. [PubMed: 23536068]

Russell FA, King R, Smillie SJ, Kodji X, Brain SD. Calcitonin gene-related peptide: physiology and pathophysiology. Physiol Rev. 2014; 94:1099–1142. [PubMed: 25287861]

Schmidt R, Schmelz M, Forster C, Ringkamp M, Torebjork E, Handwerker H. Novel classes of responsive and unresponsive C nociceptors in human skin. J Neurosci. 1995; 15:333–341. [PubMed: 7823139]

Smith-Edwards KM, DeBerry JJ, Saloman JL, Davis BM, Woodbury CJ. Profound alteration in cutaneous primary afferent activity produced by inflammatory mediators. Elife. 2016; 5

Song H, Yao E, Lin C, Gacayan R, Chen MH, Chuang PT. Functional characterization of pulmonary neuroendocrine cells in lung development, injury, and tumorigenesis. Proc Natl Acad Sci U S A. 2012; 109:17531–17536. [PubMed: 23047698]

Usoskin D, Furlan A, Islam S, Abdo H, Lonnerberg P, Lou D, Hjerling-Leffler J, Haeggstrom J, Kharchenko O, Kharchenko PV, et al. Unbiased classification of sensory neuron types by large-scale single-cell RNA sequencing. Nat Neurosci. 2015; 18:145–153. [PubMed: 25420068]

Vrontou S, Wong AM, Rau KK, Koerber HR, Anderson DJ. Genetic identification of C fibres that detect massage-like stroking of hairy skin in vivo. Nature. 2013; 493:669–673. [PubMed: 23364746]

Weyer AD, O'Hara CL, Stucky CL. Amplified Mechanically Gated Currents in Distinct Subsets of Myelinated Sensory Neurons following In Vivo Inflammation of Skin and Muscle. J Neurosci. 2015; 35:9456–9462. [PubMed: 26109668]

Wu H, Williams J, Nathans J. Morphologic diversity of cutaneous sensory afferents revealed by genetically directed sparse labeling. Elife. 2012; 1:e00181. [PubMed: 23256042]

Yarmolinsky DA, Peng Y, Pogorzala LA, Rutlin M, Hoon MA, Zuker CS. Coding and Plasticity in the Mammalian Thermosensory System. Neuron. 2016

Zylka MJ, Rice FL, Anderson DJ. Topographically distinct epidermal nociceptive circuits revealed by axonal tracers targeted to Mrgprd. Neuron. 2005; 45:17–25. [PubMed: 15629699]

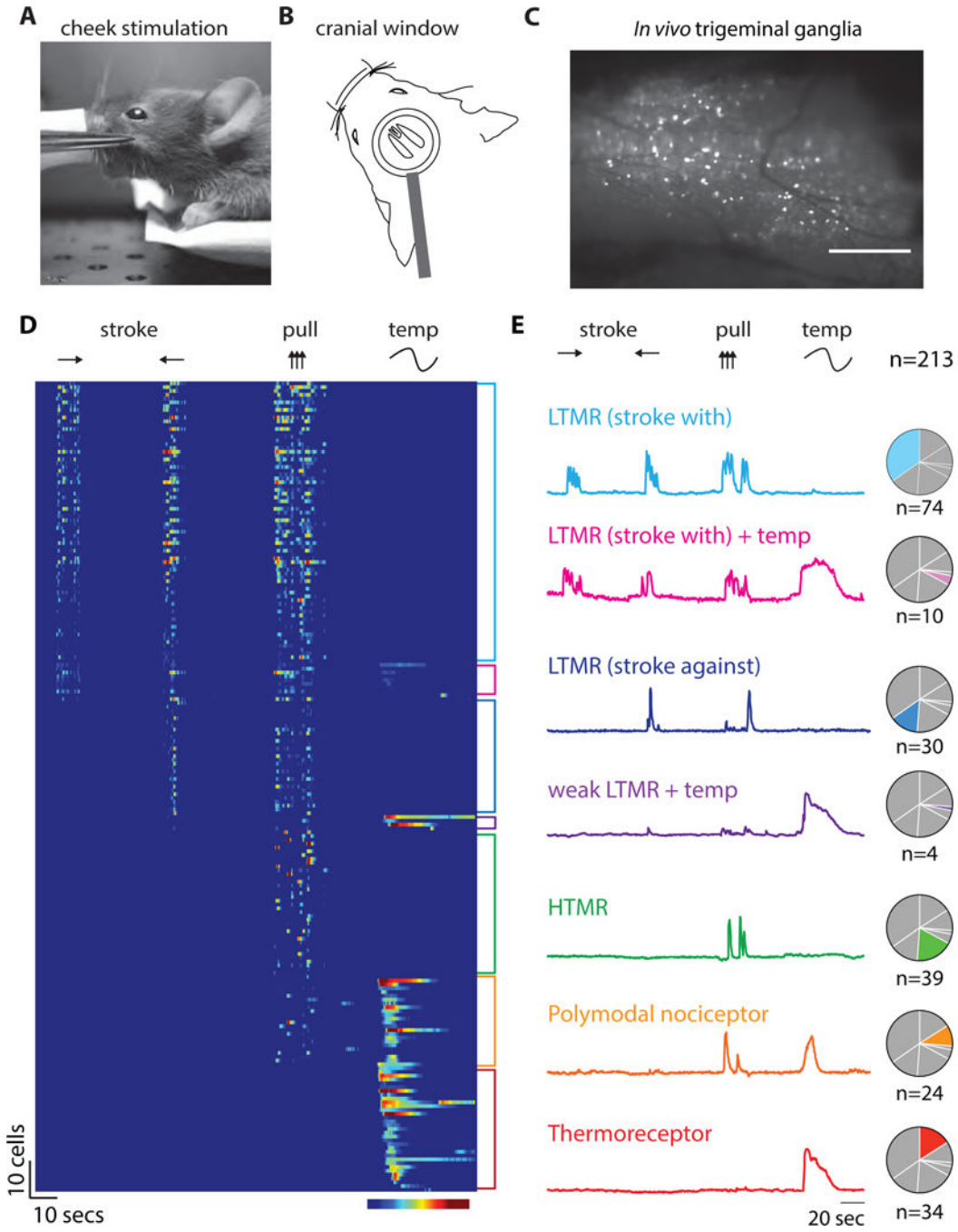

Figure 1. In vivo calcium imaging in Trpv1^{lin}-GCaMP6f mice

(A) Example of hair pull stimulation of hairy skin (cheek) using forceps. **(B)** Diagram of the trigeminal imaging preparation illustrating the cranial window and head fixation used for the in vivo imaging experiments. **(C)** Epifluorescent image of a trigeminal ganglion from a Trpv1^{lin}-GCaMP6f mouse demonstrating the visualization of responses evoked by hair pull; scale bar = 500 μm. **(D)** Heat map showing all Trpv1^{lin}-GCaMP6f neurons recorded (n=213; N=3). Stroking in both directions (with and against), hair pull, and a temperature ramp (25°C >47°C >12°C. Color range = 10–60% Δf/F. **(E)** Representative Δf/F traces for each

type of sensory neuron observed, normalized to maximum. Pie charts show the relative abundance of each class. LTMR= low threshold mechanoreceptor and HTMR=high threshold mechanoreceptor.

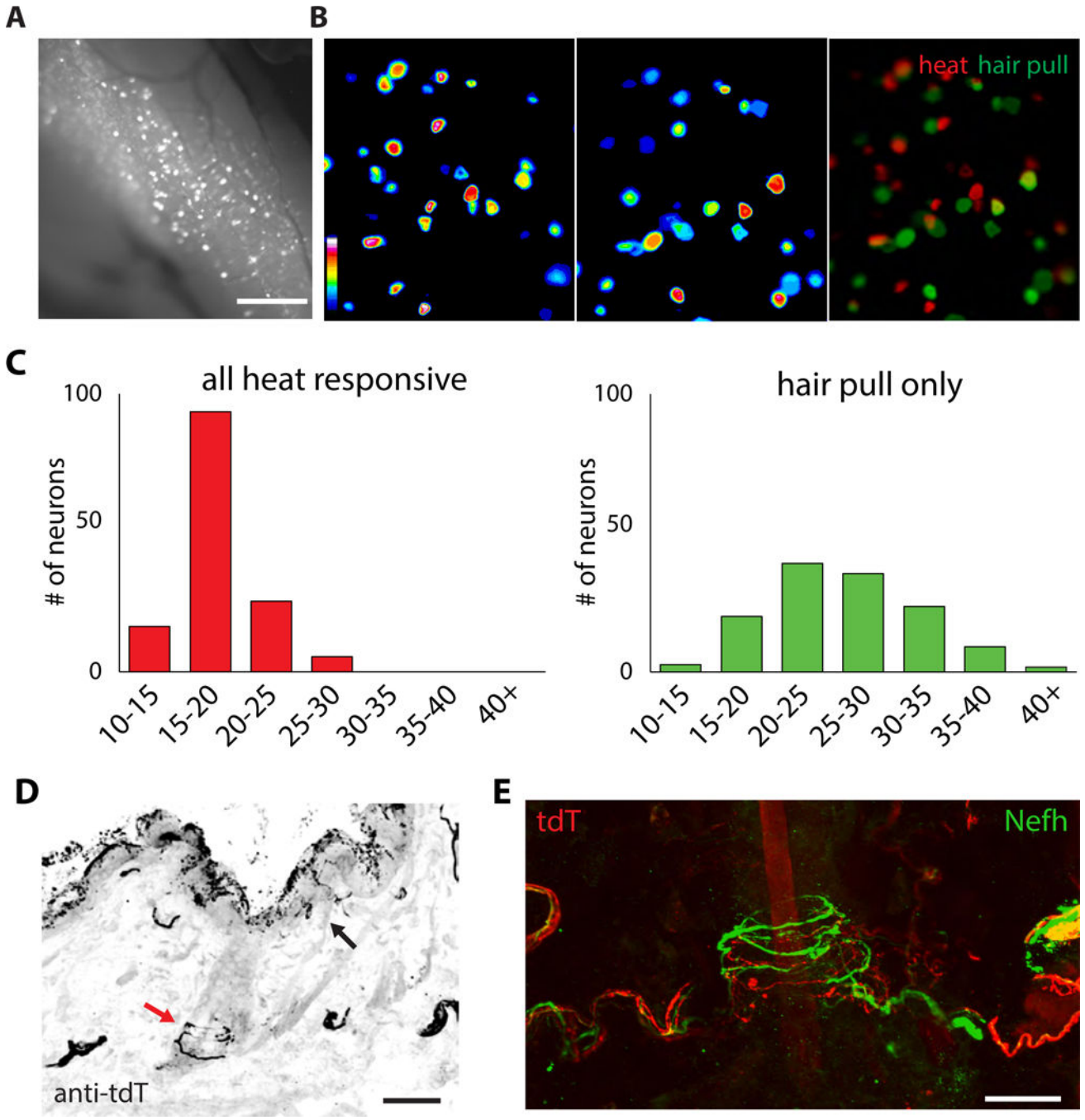

Figure 2. In vivo imaging reveals distinct classes of Calca neurons

(A) Epifluorescent image of a trigeminal ganglion from a Calca-GCaMP6f mouse demonstrating the visualization of responses evoked by hair pull; scale bar = 500 μm. **(B)** Calcium increases in a single field of view to heat (>40°C, left) and hair pulling (middle). The two responses are overlaid in pseudocolor (red for heat and green for hair pull) to reveal cells that respond to either one or both stimuli; scale bar = 100 μm. **(C)** Frequency histogram of all neurons responding to heat (red, left panel) and hair pull (green, right panel) ordered by soma size (5 mm bins). Heat responsive neurons have small diameters. By contrast Calca

neurons responding only to hair pull have larger cell diameters. **(D)** Section of hairy skin from a Calca-tdT mouse stained with anti-tdTomato showing free nerve endings (black arrow) just below the dermal surface, as well as circumferential endings (red arrow) surrounding a hair follicle. Scale = 50 μm. **(E)** An example of two types of circumferential endings at a single hair, those labeled by tdTomato (red) that originate from Calca neurons and a separate type that is labeled by Nefh (green); scale bar = 25 μm.

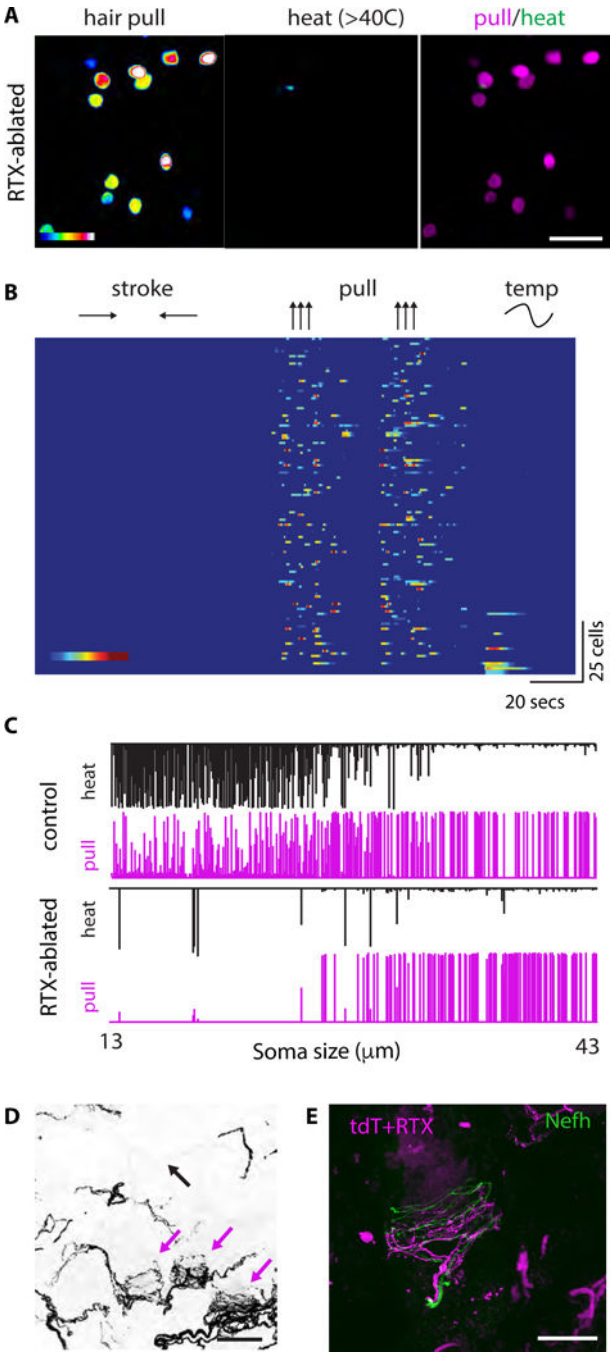

Figure 3. Medium diameter Calca-neurons are HTMRs that make circumferential endings

(A–B) Treatment with the potent Trpv1 agonist RTX ablates heat responsive Calca neurons thus isolating a class of HTMRs. **(A)** Calcium increases in a single field of view to hair pull (left) and heat (>40°C, middle). The two responses are overlaid in pseudocolor (green for heat and magenta for hair pull) to reveal cells that only respond to hair pull (scale bar = 100 μm). **(B)** Raster plots of all neurons analyzed from Calca-GCaMP6f mice treated with RTX (n=136; N=5). Cells are ordered by size (largest to smallest, top to bottom). Color scale range = 20–100% Δf/F. **(C)** Top: Responsive Calca-GCaMP6f neurons (n= 277 neurons

tested for temperature response) are sorted by soma size from smallest to largest (range = 13 μm – 43 μm). For each cell, the relative responses to heat (black bar, top) and to pull (magenta bar, bottom) are shown. The responses are normalized to the maximum of their combined peak response. Bottom: RTX-treated mice have a selective loss of smaller heat-sensitive neurons. **(D)** Circumferential endings (magenta arrows) in hairy skin persist after RTX treatment. Free nerve endings are absent below the epidermal surface (black arrow, compare with Figure 2E). Scale = 50 μm **(E)** Nefh (green) negative circumferential endings (magenta) persist after RTX treatment scalebar = 25 μm.

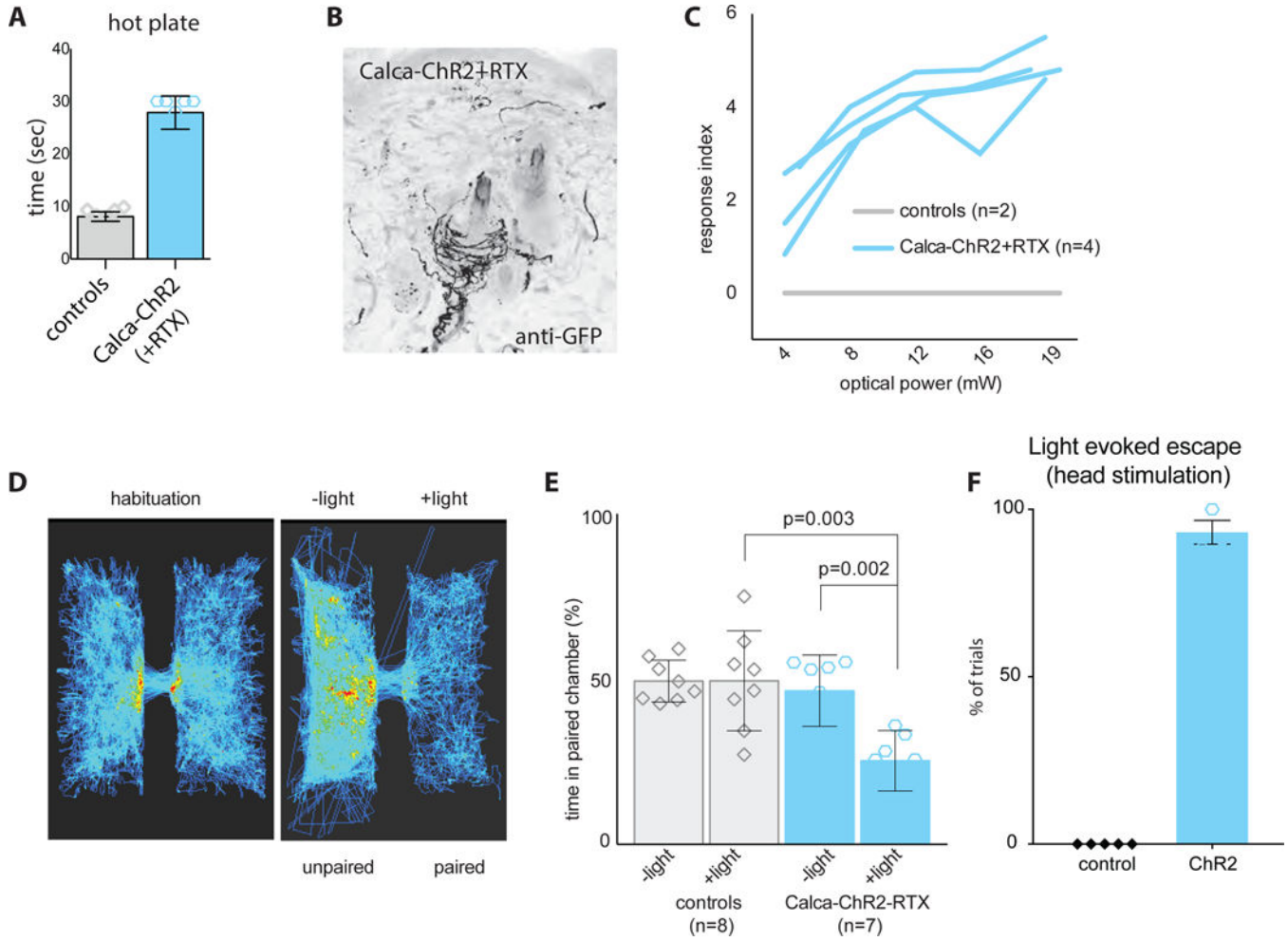

Figure 4. Activation of Circ-HTMRs is aversive

Calca-ChR2 mice were treated with RTX to isolate the Circ-HTMR population and their behavior to blue light stimulation recorded. **(A)** Hot plate assay confirmed that RTX treated animals (blue, n=7) are not responsive to noxious temperatures (55°C). Latency to hind leg withdrawal was measured with a 30 second cutoff. Controls (grey, n=6) reacted within 10 s to the heat stimulus. **(B)** Immunostaining of hairy skin from Calca-ChR2 mice revealed circumferential endings around hair shafts persist following administration of RTX. **(C)** The increasing magnitude of nocifensive behaviors observed (flinch, hunch, one leg up, two legs up, three legs up, jump) was scored with a response index ranging from 1–6. The response index for each mouse was plotted for increasing amounts of optical power. **(D)** Automated video tracking (depicted as heat maps) of a mouse moving within and across two adjoining chambers connected by a small opening. Mice equally explored both chambers in habituation trials but rapidly developed place aversion when one side was paired with focused blue light stimulation streaked across the back (trial = 20 mins). **(E)** Quantification of time spent in the paired chamber showing that Calca-ChR2-RTX mice (blue bars) develop real time place aversion (RTPA) while control mice that lack ChR2 expression (grey bars) do not develop a preference. Compare the habituation period (−light) with the test period (+light). Significance determined using an unpaired t-test. **(F)** Quantification of escape

behavior of Calca-ChR2-RTX mice to light stimulation on top of the head. Control mice that lack ChR2 expression do not show escape behavior to light simulation.

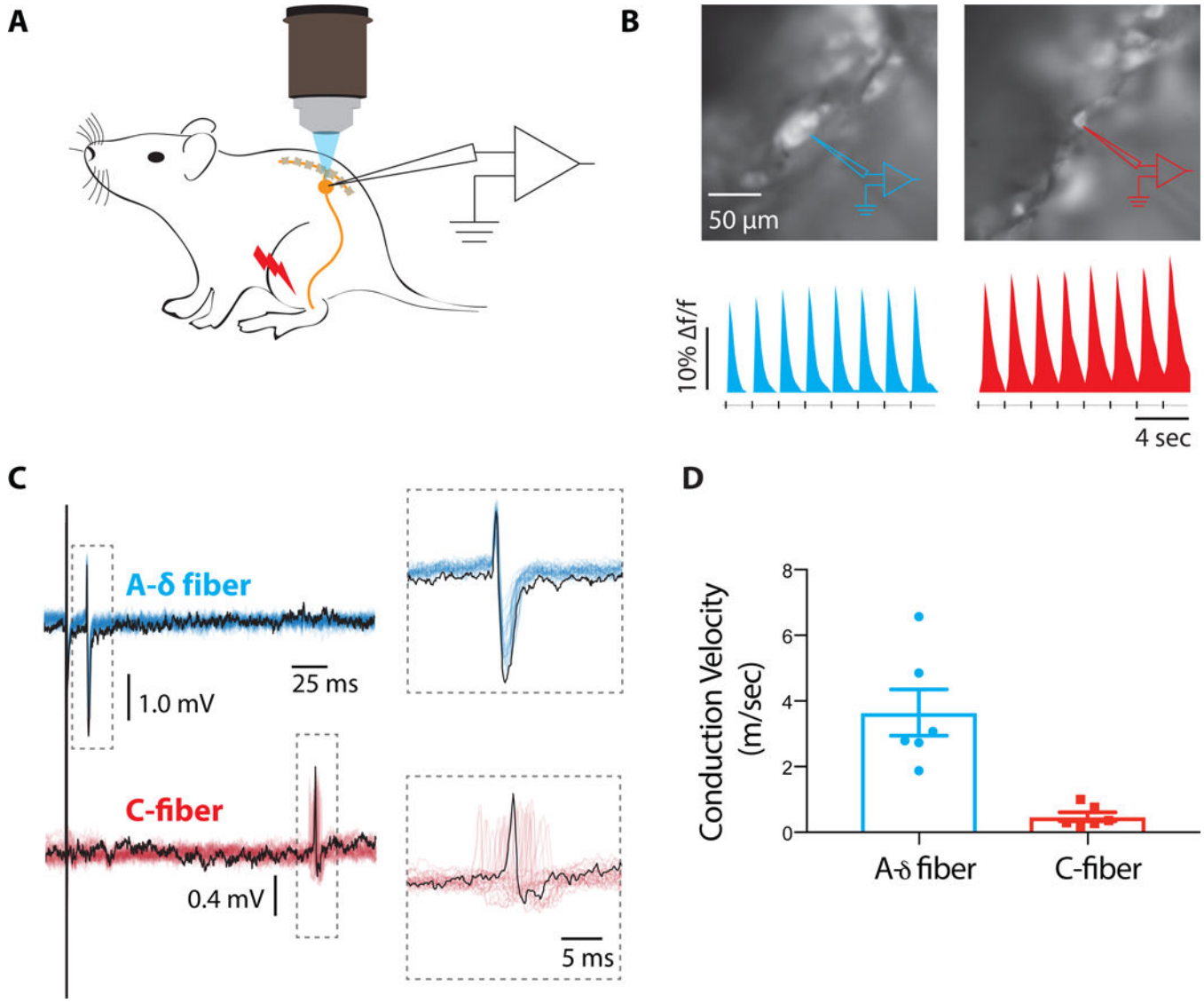

Figure 5. Extracellular recordings of action potentials revealed Circ-HTMRs have conduction velocities (CVs) in the Aδ range

(A) Schematic drawing of the in-vivo experimental setup, whereby peripherally evoked action potentials were recorded simultaneously by calcium imaging and by an extracellular sharp electrode. **(B)** Fluorescence images of medium diameter (top left) and small diameter (top right) Calca neurons in the DRG, overlaid with drawings of extracellular recording pipettes (in color code). Calcium responses to electrical stimulation delivered to the hairy skin of the leg (bottom traces). Each transient was evoked by a single action potential simultaneously measured with the recording pipette. **(C)** Extracellular recordings of action potentials from the same neurons in **A** and **B** showing large difference in response latency (electrical stimulus indicated by black line over traces). The boxed region shows an expanded time scale. **(D)** Plots of CV measurements from six medium diameter neurons with CVs in the A-δ fiber range (means: 3.6 ± 0.47 m/s, 34.8 ± 2.2 um), and six small diameter neurons with CVs in the C-fiber range (means: 0.71 ± 0.13 m/s, 19.8 ± 1.5 um).

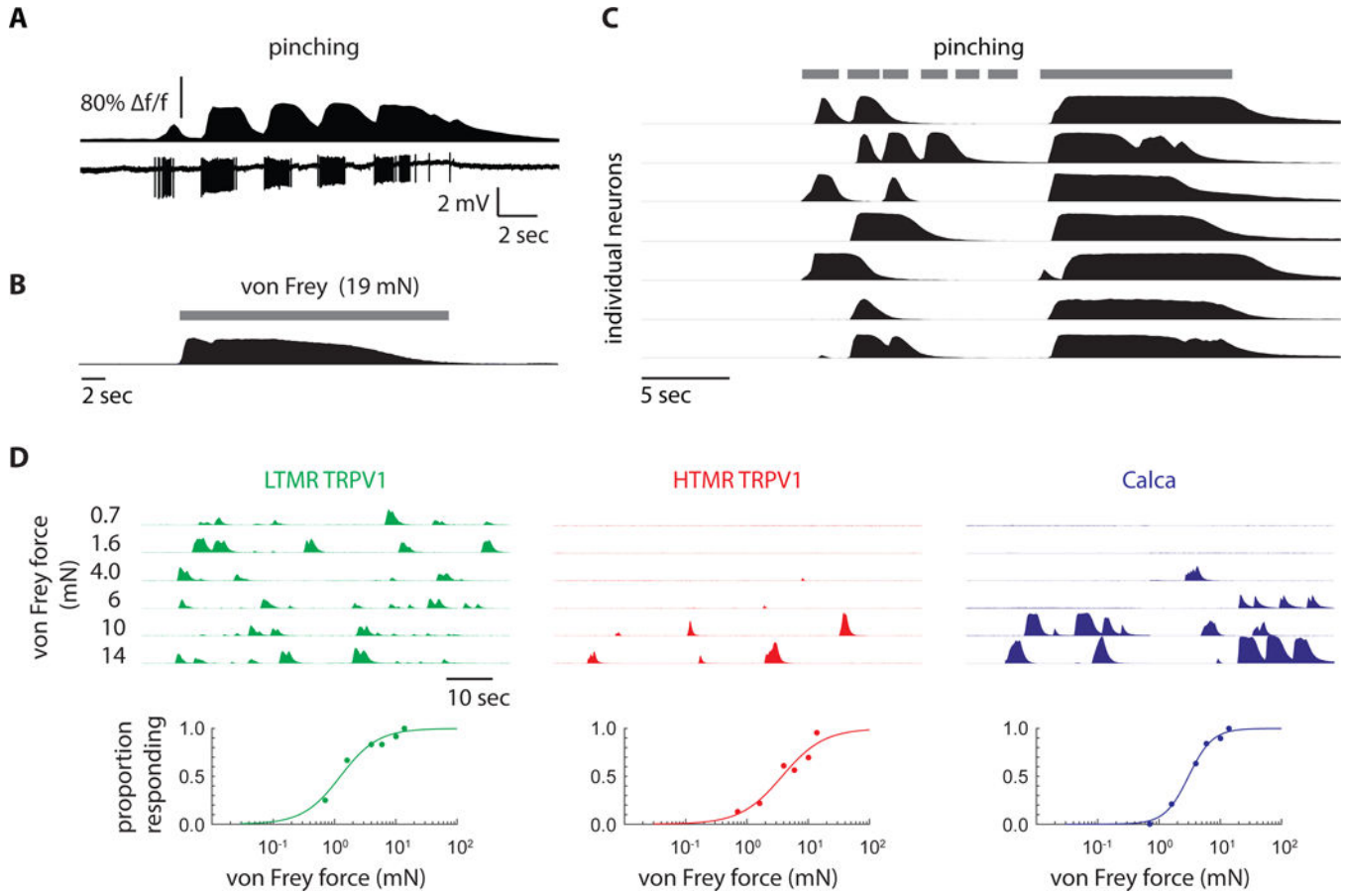

Figure 6. Circ-HTMRs display slow adaption and require high mechanical forces for activation

(A) Simultaneous calcium imaging and electrical recording from a Calca neuron in the DRG showed slow adaptation to sustained pinching. **(B)** Sustained von Frey stimulation of the cheek revealed slowly adapting calcium responses, as seen with pinching. **(C)** Calcium responses from 7 individual Circ-HTMRs (rows of black traces) in the TG that responded repeatedly to pinching. Grey bar indicates pinching epochs. Note that the neurons continuously responded to sustained stimuli (>10 s) demonstrating they are slowly adapting. **(D)** Calcium responses in TG to von Frey stimulation at increasingly higher forces (from top to bottom) from a representative TRPV1^{lin} LTMR, a TRPV1^{lin} HTMR, and a Calca neuron color coded in green, red, and blue respectively. Proportion of neurons activated are plotted (below) against von Frey force.

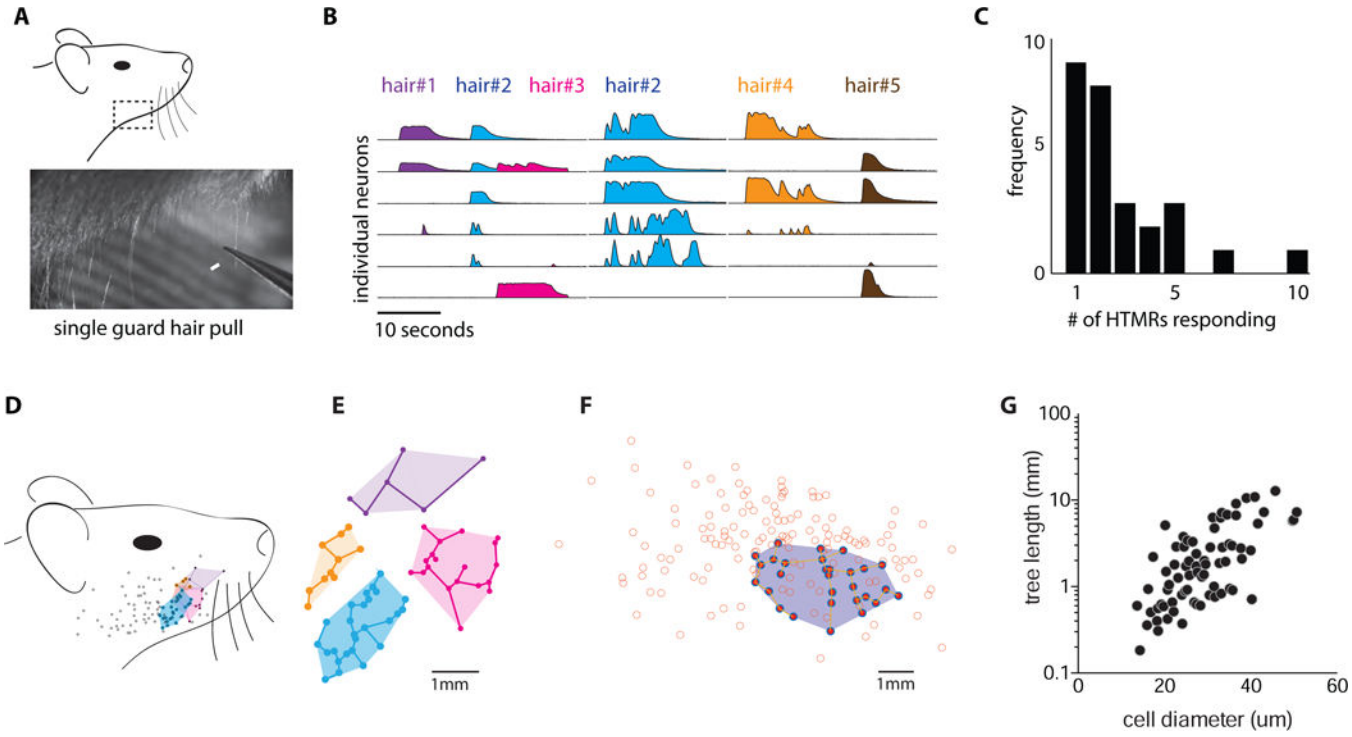

Figure 7. Circ-HTMRs are activated by single hair pull and have large, partially overlapping receptive fields

(A) Diagram of the area of hairy skin (lower cheek, boxed area) targeted for single hair pull experiments. Still frame from a high-speed video (bottom panel) shows the pulling of a single guard hair using fine forceps (arrow). **(B)** Responses of 6 individual neurons to the pulling of 5 guard hairs in a single trial. Colors represent the hair that was pulled. Note that the same combination of cells responded to hair #2 (blue) each time it was pulled. **(C)** Histogram summarizing the number of neurons activated by single hair pull events across experiments (n=27). **(D)** Receptive field maps were generated for individual neurons by charting sites of von Frey punctate stimulation (10 mN). Color-coded dots correspond to responses and grey dots represent no response. The responses for 4 individual neurons are overlaid to illustrate their partially overlapping receptive fields. **(E)** Example of a Circ-HTMR receptive field mapped showing sensitive sites (filled violet circles) and insensitive sites (open orange circles). The shortest span tree (see methods) in the shaded region surrounds insensitive sites. **(F)** To quantify the receptive field area, responsive sites were connected by shortest span tree (see methods). **(G)** The length of each tree was plotted against cell diameter showing that larger cells have larger receptive areas.